Fate of magnetic impurity induced states in a non-Hermitian *s*-wave superconductor

Chunhui Zhang [1,*] and Li Sheng[2]

[1]*College of Physics and Electronic Science, Hubei Normal University, Huangshi 435002, China*
[2]*National Laboratory of Solid State Microstructures, Department of Physics,*
and Collaborative Innovation Center of Advanced Microstructures, Nanjing University, Nanjing 210093, China

Recently, the non-Hermitian system has attracted great attention. However, the interplay between the non-Hermiticity and impurities in superconductors remains to be explored. In this work, we investigate the magnetic impurity chain on a three-dimensional non-Hermitian *s*-wave superconductor with the imbalanced pairing term. For the Yu-Shiba-Rusinov (YSR)-type state, we find that their fate is determined by the generalized in-gap nature of these states: These in-gap states and related topological phases survive only when the effective superconducting gap exists. With the increasing strength of the non-Hermitian part of the pairing term, the host superconductor is lead to a non-Hermitian gapless phase with exceptional surfaces, while these in-gap states and topological phases disappear. Our work generalizes the in-gap state nature of the YSR state to the non-Hermitian superconductor and reveals the relation between the exceptional surfaces and the YSR-type state, which provides a minimal starting point to explore the interplay between the non-Hermiticity and magnetic impurities in the *s*-wave superconductor.

I. INTRODUCTION

The past few years have witnessed the growing attention and efforts paid to non-Hermitian physics [1]. In non-Hermitian physics, the exceptional points (EPs) are a very important topic [2]: At these singularity points, the eigenvalues are degenerate and the eigenstates coalesce [2,3]. Furthermore, the EPs are involved in understanding $\mathcal{PT}$-symmetric quantum mechanics [4–14] and bulk Fermi arcs [3,15–22] in non-Hermitian systems. Finally, EPs have been found in many physical systems including open quantum systems [23–33], the condensed-matter systems with self-energy effects [3,15–18,20,34–42], and optical systems [43–52].

In condensed-matter physics, impurity is almost unavoidable and plays very important roles. For instance, the impurity in metals introduces the Friedel oscillation of the electron density [53,54]. As for the magnetic impurity chain in an *s*-wave superconductor, every single magnetic impurity also introduces the Yu-Shiba-Rusinov (YSR) bound state in the superconducting (SC) gap [55–57]. When these impurities are close to one another, these bound states hybridize and can form bands. Based on these results, recent studies have pointed out that the magnetic impurity chain has helical spin textures, and bands from the hybridization of the YSR states are topologically nontrivial [58–60]. Thus, the YSR chain [61–68] in an *s*-wave superconductor can be applied to realize the topological superconductivity [69–75]. To our best knowledge, YSR states are in-gap states. Then, if the SC gap decreases or vanishes, what happens to these in-gap states? This question is important in non-Hermitian superconductors

because the non-Hermitian part of the SC term can decrease the SC gap and introduce the exceptional manifolds [24,76–79]. Furthermore, since bands of the helical YSR chain are formed by these YSR bound states [60], it is also interesting to study the effect of the non-Hermitian SC term on bands and topological phases of the helical YSR chain.

In this paper, we investigate a magnetic impurity chain on a three-dimensional (3D) imbalanced *s*-wave superconductor as shown in Fig. 1. We find that the fates of YSR-type states are determined by their generalized in-gap state nature: These YSR-type states and related topological bands survive as long as the effective SC gap still exist. And the non-Hermiticity changes the effective coherence length, which modifies the phase diagrams of the impurity chain. Once the effective SC gap is destroyed by the non-Hermiticity, these YSR-type states and related bands are not allowed to exist in the non-Hermitian gapless phase with exceptional surfaces.

This paper is organized as follows. In Sec. II we review the spectrum of a 3D imbalanced *s*-wave superconductor and show that this model can be gapped or gapless according to the strength of the non-Hermitian term. Then, in Sec. III, by solving the eigenstate at the position of the single impurity, we show that the generalized in-gap nature of a YSR-type state determines its fate. Next, in Sec. IV we consider the helical magnetic impurity chain in a superconductor with imbalanced *s*-wave superconductivity. After introducing the projection method in Sec. IV A, we show and discuss the resulting Hamiltonian and the corresponding Bloch spectrum in Sec. IV B. Then, for the non-Hermitian gapless phase in the host superconductor, in Sec. IV C we explain the reason why YSR-type bands cannot be formed. In Sec. IV D, for the gapped phase, we give the phase diagrams and show that the non-Hermiticity affects the topological phase by changing

---

*zhangchunhui@hbnu.edu.cn
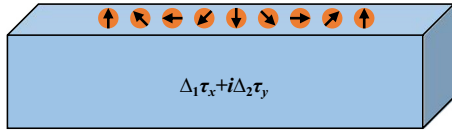
FIG. 1. Schematic of the helical magnetic impurity chain on a 3D superconductor with the imbalanced s-wave pairing potential $\Delta_1\tau_x + i\Delta_2\tau_y$. Each magnetic impurity is represented as an orange circle. The small black arrows indicate the spin direction of each magnetic impurity. The blue box represents the host superconductor.

the effective coherence length. Finally, in Sec. V we discuss possible experimental regimes about the related model with an imaginary SC pairing term and we give a summary.

II. THE SPECTRUM OF THE IMBALANCED s-WAVE SUPERCONDUCTOR

Before discussing the magnetic impurity, we review the spectrum of the 3D imbalanced s-wave superconductor. Without the non-Hermitian superconductivity, the system can be described as the following free electron gas model:

$$\epsilon_k = \frac{\boldsymbol{k}^2}{2m} - \mu. \tag{1}$$

Here, the chemical potential $\mu \geqslant 0$ and m is the effective mass. Then, under the Nambu basis

$$\Psi_{\boldsymbol{k}} = (c_{\mathbf{k},\uparrow}, c_{\mathbf{k},\downarrow}, c_{-\mathbf{k},\downarrow}^\dagger, -c_{-\mathbf{k},\uparrow}^\dagger)^T, \tag{2}$$

the imbalanced s-wave pairing term is

$$\Delta_{\boldsymbol{k}} = \Delta_1\tau_x + i\Delta_2\tau_y, \tag{3}$$

where $\Delta_1 > 0$ denotes the strength of the Hermitian term, and the non-Hermiticity in our model is introduced by $\Delta_2 > 0$. We note that the effects of the imbalanced s-wave superconductivity with $\Delta_1 = 0$ [76,78,79] and an imbalanced p-wave pairing potential [77,80,81] have been investigated recently. Motivated by these previous works about the non-Hermitian superconductivity, the imbalanced s-wave pairing potential $\Delta_{\mathbf{k}}$ is considered in our work.

Then, by combing Eqs. (1) and (3) in the Nambu space, we obtain the following Bogoliubov–de Gennes(BdG) Hamiltonian:

$$H_0(\mathbf{k}) = \epsilon_{\boldsymbol{k}}\tau_z + \Delta_{\boldsymbol{k}} = \epsilon_{\boldsymbol{k}}\tau_z + \Delta_1\tau_x + i\Delta_2\tau_y, \tag{4}$$

where the Pauli matrix $\tau_{i=x,y,z}$ acts on the Nambu degree of freedom. Similar to the imbalanced p-wave superconductor [77], Eq. (4) can be transformed into a balanced s-wave superconductor model,

$$\tilde{H}_0(\mathbf{k}) = \hat{\eta}H_0(\mathbf{k})\hat{\eta}^{-1} = \epsilon_{\boldsymbol{k}}\tau_z + \sqrt{\Delta_1^2 - \Delta_2^2}\,\tau_x, \tag{5}$$

with the following transformation matrix:

$$\hat{\eta} = \begin{pmatrix} \left(\frac{\Delta_1 - \Delta_2}{\Delta_1 + \Delta_2}\right)^{\frac{1}{4}} & 0 \\ 0 & \left(\frac{\Delta_1 + \Delta_2}{\Delta_1 - \Delta_2}\right)^{\frac{1}{4}} \end{pmatrix}. \tag{6}$$
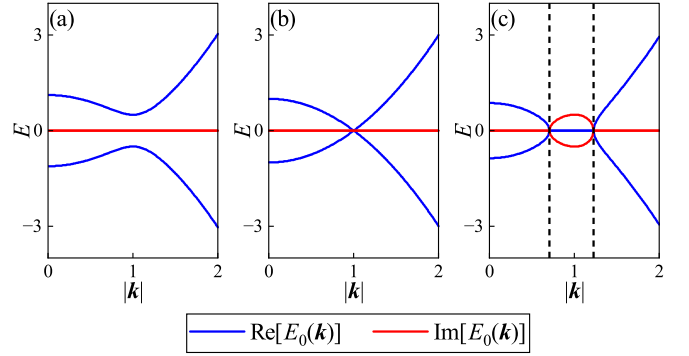
FIG. 2. Real and imaginary parts of $E_0(\boldsymbol{k})$ as functions of $|\boldsymbol{k}|$. Panel (a), (b), and (c) correspond with the spectrums with $1 - \gamma^2 = 0.25$, 0, and -0.25, correspondingly. The blue (red) lines denote real (imaginary) parts of $E_{0,\pm}(\boldsymbol{k})$. The dashed lines denote the exceptional surfaces given by Eq. (9). Other parameters are $m = 0.5$ and $\mu = 1.0$.

Next, we consider the spectrum of $H_0(\boldsymbol{k})$ [or $\tilde{H}_0(\boldsymbol{k})$], which is

$$E_{0,\pm}(\mathbf{k}) = \pm\sqrt{\epsilon_{\mathbf{k}}^2 + M_\Delta^2}, \tag{7}$$

where

$$M_\Delta = \sqrt{\Delta_1^2 - \Delta_2^2} = \Delta_1\sqrt{1 - \gamma^2} \tag{8}$$

and $\gamma = \Delta_2/\Delta_1$. In Fig. 2 we show $\text{Re}[E_{0,+}(\boldsymbol{k})]$ and $\text{Im}[E_{0,+}(\boldsymbol{k})]$ as functions of $|\boldsymbol{k}|$. When $0 < \gamma < 1$, M_Δ is real, and the SC gap still exists in Fig. 2(a). Then, Fig. 2(b) shows that $M_\Delta = 0$ and the SC gap closes if $\gamma = 1$. Finally, for the $\gamma > 1$ case, M_Δ becomes an imaginary number, and the model is in a gapless phase with exceptional surfaces [see Fig. 2(c)]. These exceptional surfaces are given by

$$|\boldsymbol{k}| = \sqrt{k_x^2 + k_y^2 + k_z^2} = [2m(\mu \pm \Delta_1\sqrt{\gamma^2 - 1})]^{\frac{1}{2}}. \tag{9}$$

In Fig. 2(c), EPs correspond to two exceptional surfaces in the k_x-k_y-k_z space.

III. MODEL WITH A SINGLE MAGNETIC IMPURITY

In this section, we consider a single magnetic impurity on a 3D imbalanced s-wave superconductor. Let us begin with the following microscopic model:

$$H = H_0(\boldsymbol{k}) - g\boldsymbol{S} \cdot \boldsymbol{\sigma}\delta(\boldsymbol{r}). \tag{10}$$

Here, $H_0(\boldsymbol{k})$ is given by Eq. (4). $g > 0$ is the strength of the exchange coupling between the classical magnetic impurity and the electron at $\boldsymbol{r} = \boldsymbol{0}$. The impurity spin $\boldsymbol{S}$ points along an arbitrary direction vector $\boldsymbol{n} = (\sin\theta\cos\phi, \sin\theta\sin\phi, \cos\phi)$ and we have

$$\boldsymbol{S} \cdot \boldsymbol{\sigma} = S\sigma_n = S(\sin\theta\cos\phi\sigma_x + \sin\theta\sin\phi\sigma_y + \cos\theta\sigma_z). \tag{11}$$

For the Hamiltonian H, its eigenequation at $\boldsymbol{r} = \boldsymbol{0}$ leads to

$$[E - H_0(\boldsymbol{k})]|\psi_R(\boldsymbol{r})\rangle = -gS\delta(\boldsymbol{r})\sigma_n|\psi_R(\boldsymbol{0})\rangle. \tag{12}$$

Here, the index R denotes the right eigenvectors in the non-Hermitian problem. Then, note that $\hat{\eta}$ does not act on the

spin degree of freedom (i.e., $\hat{\eta}$ commutates with the $\boldsymbol{\sigma}_n$); we multiply $\hat{\eta}$ from the left of Eq. (12) and obtain

$$\hat{\eta}[E - H_0(\boldsymbol{k})]\hat{\eta}^{-1}\hat{\eta}|\psi_R(\boldsymbol{r})\rangle = -gS\delta(\boldsymbol{r})\boldsymbol{\sigma}_n\hat{\eta}|\psi_R(\boldsymbol{0})\rangle. \quad (13)$$

Next, with Eq. (5), we have

$$(E - \epsilon_k\tau_z - M_\Delta\tau_x)|\psi'(\boldsymbol{r})\rangle = -gS\delta(\boldsymbol{r})\boldsymbol{\sigma}_n|\psi'(\boldsymbol{0})\rangle, \quad (14)$$

with $|\psi'(\boldsymbol{r})\rangle = \hat{\eta}|\psi_R(\boldsymbol{r})\rangle$. This eigenequation looks quite similar to the Hermitian model. However, there is a difference between Eq. (14) and the Hermitian case: The effective pairing term is M_Δ. As we have discussed in Sec. II, this term is zero or an imaginary number when the gap of a host superconductor closes.

Now, according to Ref. [60], by multiplying $[E - \epsilon_{\boldsymbol{k}}\tau_z - M_\Delta\tau_x]^{-1}$ from the left of Eq. (14) and making the Fourier transformation, we obtain

$$\begin{aligned}|\psi'_{\boldsymbol{k}}\rangle &= \frac{-gS\boldsymbol{\sigma}_n}{E - \epsilon_k\tau_z - M_\Delta\tau_x}|\psi'(\boldsymbol{0})\rangle \\ &= \frac{-gS[E + \epsilon_k\tau_z + M_\Delta\tau_x]}{E^2 - \epsilon_{\boldsymbol{k}}^2 - M_\Delta^2}\boldsymbol{\sigma}_n|\psi'(\boldsymbol{0})\rangle, \quad (15)\end{aligned}$$

which leads to

$$[\boldsymbol{1} + J_0(E)\boldsymbol{\sigma}_n]|\psi'(\boldsymbol{0})\rangle = 0, \quad (16)$$

with

$$\begin{aligned}J_0(E) &= \int \frac{d\boldsymbol{k}}{(2\pi)^3} \frac{gS[E + \epsilon_k\tau_z + M_\Delta\tau_x]}{E^2 - \epsilon_{\boldsymbol{k}}^2 - M_\Delta} \\ &= \nu_0 \int d\epsilon_k \frac{gS[E + \epsilon_k\tau_z + M_\Delta\tau_x]}{(\epsilon_{\boldsymbol{k}} + xi)(\epsilon_{\boldsymbol{k}} - xi)}, \quad (17)\end{aligned}$$

where $x = \sqrt{M_\Delta^2 - E^2}$ and ν_0 is the density of states of the free electron gas at the Fermi level. When

$$\text{Re}(x) = \text{Re}\left(\sqrt{M_\Delta^2 - E^2}\right) \neq 0, \quad (18)$$

Eq. (17) becomes [82]

$$J_0(E) = -\frac{\alpha(E\tau_0 + M_\Delta\tau_x)}{\sqrt{M_\Delta^2 - E^2}}, \quad (19)$$

with $\alpha = gS\pi\nu_0$. Note that Eq. (16) has nontrivial solutions if $\det[\boldsymbol{1} + J_0(E)\boldsymbol{\sigma}_n] = 0$, i.e.,

$$\left(1 \pm \frac{\alpha E}{\sqrt{M_\Delta - E^2}}\right)^2 - \frac{\alpha^2 M_\Delta^2}{M_\Delta^2 - E^2} = 0. \quad (20)$$

We can solve the following single impurity spectrum:

$$E_\pm = \pm M_\Delta \frac{1 - \alpha^2}{1 + \alpha^2} = \pm\Delta_1\sqrt{1 - \gamma^2}\frac{1 - \alpha^2}{1 + \alpha^2}. \quad (21)$$

If $\gamma = 0$, Eq. (21) reduces to the spectrum of the Hermitian YSR bound state [55–57,60].

Next, by substituting $E_\pm$ into Eq. (17), we obtain the following eigenvectors:

$$|\psi'_+(\boldsymbol{0})\rangle = \frac{1}{\sqrt{C}}\begin{pmatrix}|\uparrow\rangle \\ |\uparrow\rangle\end{pmatrix}, \quad |\psi'_-(\boldsymbol{0})\rangle = \frac{1}{\sqrt{C}}\begin{pmatrix}|\downarrow\rangle \\ -|\downarrow\rangle\end{pmatrix}, \quad (22)$$
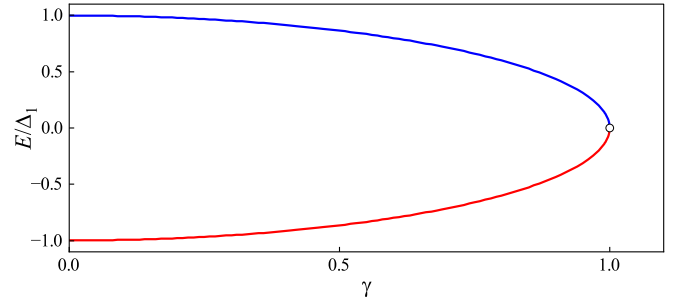
FIG. 3. Single impurity spectra $E_\pm$ in Eq. (21) as functions of γ. The blue (red) solid line corresponds to E_+ (E_-). The point at $(\gamma, E/\Delta_1) = (0, 0)$ denotes that no YSR-type state exist since the host model becomes gapless. Another parameter is $\alpha = 0.95$.

with the factor C and the eigenvectors of $\boldsymbol{\sigma}_n$:

$$|\uparrow\rangle = \begin{pmatrix}\cos\frac{\theta}{2} \\ \sin\frac{\theta}{2}e^{i\phi}\end{pmatrix}, \quad |\downarrow\rangle = \begin{pmatrix}\sin\frac{\theta}{2}e^{-i\phi} \\ -\cos\frac{\theta}{2}\end{pmatrix}. \quad (23)$$

Since $|\psi'(\boldsymbol{r})\rangle = \hat{\eta}|\psi_R(\boldsymbol{r})\rangle$, the right-eigenvectors in Eq. (12) are

$$\begin{aligned}|\psi_{R,+}(\boldsymbol{0})\rangle &= \hat{\eta}^{-1}|\psi'_+(\boldsymbol{0})\rangle = \frac{\hat{\eta}^{-1}}{\sqrt{C}}\begin{pmatrix}|\uparrow\rangle \\ |\uparrow\rangle\end{pmatrix}, \\ |\psi_{R,-}(\boldsymbol{0})\rangle &= \hat{\eta}^{-1}|\psi'_-(\boldsymbol{0})\rangle = \frac{\hat{\eta}^{-1}}{\sqrt{C}}\begin{pmatrix}|\downarrow\rangle \\ -|\downarrow\rangle\end{pmatrix}, \quad (24)\end{aligned}$$

and the corresponding left-eigenvectors are (see Appendix A)

$$\begin{aligned}|\psi_{L,+}(\boldsymbol{0})\rangle &= \hat{\eta}|\psi'_+(\boldsymbol{0})\rangle = \frac{\hat{\eta}}{\sqrt{C}}\begin{pmatrix}|\uparrow\rangle \\ |\uparrow\rangle\end{pmatrix}, \\ |\psi_{L,-}(\boldsymbol{0})\rangle &= \hat{\eta}|\psi'_-(\boldsymbol{0})\rangle = \frac{\hat{\eta}}{\sqrt{C}}\begin{pmatrix}|\downarrow\rangle \\ -|\downarrow\rangle\end{pmatrix}, \quad (25)\end{aligned}$$

with the spectrum given by Eq. (21). For these right- and left-eigenvectors, the factor $C = 2$ can be obtained by the binormalized condition $\langle\psi_{L,+}(\boldsymbol{0})|\psi_{R,+}(\boldsymbol{0})\rangle = \langle\psi_{L,-}(\boldsymbol{0})|\psi_{R,-}(\boldsymbol{0})\rangle = 1$. Now, we discuss the results of the model with the single impurity. The single impurity spectrum, Eq. (21), as the function of γ is plotted in Fig. 3. We find that as γ increases, $|E_\pm|$ decreases. Meanwhile, we exclude the point $(\gamma, E/\Delta_1) = (0, 0)$ in this spectrum. To illustrate this result, we substitute Eq. (21) into Eq. (18), which yields

$$\begin{aligned}\text{Re}\left(\sqrt{M_\Delta^2 - E^2}\right) &= \pm\frac{2\alpha}{1 + \alpha^2}\text{Re}(M_\Delta) \\ &= \pm\frac{2\Delta_1\alpha}{1 + \alpha^2}\text{Re}(\sqrt{1 - \gamma^2}) \neq 0. \quad (26)\end{aligned}$$

Here, Eq. (26) is satisfied if $\gamma \in [0, 1)$. This result is a generalization of the in-gap nature of the YSR state: *The magnetic impurity-induced state is protected by the effective gap M_Δ of the host superconductor. As long as the gap is destroyed by the non-Hermiticity, these states cannot exist.* For this reason, the eigenstates in Eqs. (24) and (25) are dubbed "YSR-type states." Meanwhile, as we have shown in Figs. 2(b) and 2(c), the host model is gapless when $\gamma \geqslant 1$, so no YSR-type state exists. At last, for the host model with $\gamma > 1$, since the exceptional surfaces accompany the non-Hermitian *gapless*

phase, we can conclude that the YSR-type state is forbidden to survive once exceptional surfaces occur in the host model.

IV. MODEL WITH A MAGNETIC IMPURITY CHAIN

Now, we consider the magnetic impurity chain on an imbalanced s-wave superconductor. Here, the spin moment of the jth magnetic impurity is $\boldsymbol{S}_j = S\boldsymbol{n}_j = S(\sin\theta_j\cos\phi_j, \sin\theta_j\sin\phi_j, \cos\theta_j)$, where $\boldsymbol{n}_j$ is a unit vector denoting the direction of the spin moment. For the helical spin textures, we have a constant $\theta_j = \theta$ and $\phi_j = 2k_h x_j$ with a pitch π/k_h. The lattice constant of the impurity chain $a = 1$, and so $x_j = j$.

In the following part, we first generalize the projection method used in Ref. [60] to the non-Hermitian eigenvectors. Then, we focus on the effective resulting Hamiltonian of this magnetic impurity chain and its spectrum. Finally, we investigate the fate of the bands and topological phases of this impurity chain on the imbalanced superconductor.

A. General formulation of the projection to the right- and left-eigenvectors

Before deriving this effective model Hamiltonian, we want to introduce the concept of projection in non-Hermitian physics. To this end, we begin with the Hermitian case. After projecting a matrix A to a set of the normalized bases $(|1\rangle, |2\rangle, \ldots |i\rangle, \ldots |N\rangle)$, the elements of the resulting matrix A' are

$$A'_{ij} = \langle i|A|j\rangle. \tag{27}$$

For non-Hermitian physics, Eq. (27) can be generalized to the right- and left-eigenvectors satisfying $\langle i, L|j, R\rangle = \langle i, R|j, L\rangle = \delta_{ij}$:

$$A'_{ij} = \langle i, L|A|j, R\rangle. \tag{28}$$

Finally, we would like to consider the right-eigenvectors $|\psi_R(\boldsymbol{r}_j)\rangle$ at the jth impurity site and the left-eigenvectors $|\psi_L(\boldsymbol{r}_i)\rangle$ at the ith site. For the imbalanced pairing term, from Eq. (28) we have

$$\begin{aligned} &\langle\psi_L(\boldsymbol{r}_i)|(\Delta_1\tau_x + i\Delta_2\tau_y)||\psi_R(\boldsymbol{r}_j)\rangle \\ &= \langle\psi'(\boldsymbol{r}_i)|[\eta(\Delta_1\tau_x + i\Delta_2\tau_y)\eta^{-1}]|\psi'(\boldsymbol{r}_j)\rangle \\ &= \langle\psi'(\boldsymbol{r}_i)|(\Delta_1^2 - \Delta_2^2)\tau_x|\psi'(\boldsymbol{r}_j)\rangle \\ &= \langle\psi'(\boldsymbol{r}_i)|M_\Delta\tau_x|\psi'(\boldsymbol{r}_j)\rangle. \end{aligned} \tag{29}$$

Equation (29) means that the non-Hermitian basis $|\psi_{R,L}(\boldsymbol{r}_i)\rangle$ can be transformed into the Hermitian one $|\psi'(\boldsymbol{r}_i)\rangle$ via the transformation matrix η. During this transformation, the imbalanced pairing term is also replaced by the balanced one, and this transformation does not change the inner product. Thus, we can derive the resulting Hamiltonian H_{eff} with the Hermitian basis and the balanced pairing term (see Appendix B).

B. Effective model of the impurity chain

Next, we give the effective Hamiltonian of the magnetic impurity chain on the non-Hermitian superconductivity. We still begin with

$$H = H_0(\boldsymbol{k}) - gS\sum_j \boldsymbol{\sigma}_{n_j}\delta(\boldsymbol{r} - \boldsymbol{r}_j). \tag{30}$$

With the transformation matrix η and Eq. (29), we can obtain the following effective Hamiltonian (see Appendix B):

$$H_{\text{eff}} = M_\Delta \begin{pmatrix} h_{\uparrow\uparrow} & \Delta_{\uparrow\downarrow} \\ \Delta_{\uparrow\downarrow}^\dagger & -h_{\uparrow\uparrow}^T \end{pmatrix}, \tag{31}$$

where the elements of the matrix, $h_{\uparrow\uparrow}$ and $\Delta_{\uparrow\downarrow}$, are

$$h_{\uparrow\uparrow,ij} = \begin{cases} (1-\alpha), & \text{if } i = j, \\ -\frac{\sin(k_F r_{ij})}{k_F r_{ij}}e^{-\frac{r_{ij}}{\xi}}\left[\cos^2\left(\frac{\theta}{2}\right)e^{ik_h x_{ij}} \right. \\ \left. + \sin^2\left(\frac{\theta}{2}\right)e^{-ik_h x_{ij}}\right], & \text{if } i \neq j, \end{cases}$$

and

$$\Delta_{\uparrow\downarrow,ij} = \begin{cases} 0, & \text{if } i = j, \\ \frac{i\cos(k_F r_{ij})}{k_F r_{ij}}e^{-\frac{r_{ij}}{\xi}}\sin\theta\sin k_h x_{ij}, & \text{if } i \neq j. \end{cases} \tag{32}$$

The resulting Hamiltonian H_{eff} has the same form as the one with the Hermitian host superconductor [60]. The only difference is that the SC gap Δ_1 is replaced by the effective one $M_\Delta = \Delta_1\sqrt{1-\gamma^2}$, which leads to a modified effective coherence strength ξ:

$$\xi = \frac{v_F}{M_\Delta} = \frac{v_F}{\Delta_1\sqrt{1-\gamma^2}} = \frac{\xi_0}{\sqrt{1-\gamma^2}}, \tag{33}$$

where $\xi_0 = v_F/\Delta_1$ is the coherence length without the non-Hermiticity.

To obtain the Bloch spectrum, we make the Fourier transformations [60]

$$h_{\uparrow\uparrow,k} = \sum_j h_{\uparrow\uparrow,ij}e^{ikx_{ij}}, \quad \Delta_{\uparrow\downarrow,k} = \sum_j \Delta_{\uparrow\downarrow,ij}e^{ikx_{ij}}, \tag{34}$$

and we obtain the corresponding Hamiltonian:

$$\begin{aligned} H_{\text{eff},k} = &\frac{M_\Delta}{2}(h_{\uparrow\uparrow,k} + h_{\uparrow\uparrow,-k})\tau_z + M_\Delta\Delta_{\uparrow\uparrow,k}\tau_x \\ &+ \frac{M_\Delta}{2}(h_{\uparrow\uparrow,k} - h_{\uparrow\uparrow,-k})\tau_0, \end{aligned} \tag{35}$$

with (see Appendix C)

$$h_{\uparrow\uparrow,k} = (1-\alpha) + \frac{1}{k_F}\left[\alpha_{k+k_h}\cos^2\frac{\theta}{2} + \alpha_{k-k_h}\sin^2\frac{\theta}{2}\right],$$

$$\alpha_k = -\left[\arctan\frac{\sin(k_F+k)}{e^{\frac{\sqrt{1-\gamma^2}}{\xi_0}} - \cos(k_F+k)} \right.$$
$$\left. + \arctan\frac{\sin(k_F-k)}{e^{\frac{\sqrt{1-\gamma^2}}{\xi_0}} - \cos(k_F-k)}\right], \tag{36}$$

and

$$\Delta_k = \frac{\sin\theta}{4k_F}\left(\beta_{k_F+k_h+k} - \beta_{k_F+k_h-k} - \beta_{k_F-k_h+k} + \beta_{k_F-k_h-k}\right),$$

$$\beta_k = -\ln\left(1 + e^{-\frac{2\sqrt{1-\gamma^2}}{\xi_0}} - 2e^{-\frac{\sqrt{1-\gamma^2}}{\xi_0}}\cos k\right). \tag{37}$$

And its spectrum is

$$E_{\pm,k} = \frac{M_\Delta}{2}(h_{\uparrow\uparrow,k} - h_{\uparrow\uparrow,-k})$$
$$\pm M_\Delta\sqrt{\Delta_{\uparrow\downarrow,k}^2 + \frac{1}{4}(h_{\uparrow\uparrow,k} + h_{\uparrow\uparrow,-k})^2}. \quad (38)$$

In the following part of this section, we discuss the different fates of the topological phase of the impurity chain in the $\gamma \geqslant 1$ and $0 < \gamma < 1$ cases.

C. The lost YSR-type bands and topological phases in the $\gamma \geqslant 1$ case

We begin with the $\gamma \geqslant 1$ case. In this case, we need to stress that the topological phase in the YSR-type chain *cannot exist* even though we can write H_{eff} with $\gamma \geqslant 1$ and calculate some results (see Appendix D).

To illustrate this point, let us consider the resulting Hamiltonian H_{eff} obtained from the projection method. As we have introduced in Sec. IV A, to complete the projection, we need a set of states, which is given by

$$[|\psi'(\mathbf{r}_1)\rangle, |\psi'(\mathbf{r}_2)\rangle, \ldots, |\psi'(\mathbf{r}_i)\rangle, \ldots, |\psi'(\mathbf{r}_N)\rangle]. \quad (39)$$

Here, each $|\psi'(\mathbf{r}_i)\rangle = \eta|\psi_R(\mathbf{r}_i)\rangle = \eta^{-1}|\psi_L(\mathbf{r}_i)\rangle$ corresponds to the YSR-type state at the ith impurity lattice. In Sec. III, we have shown that the single YSR-type state cannot exist when $\gamma \geqslant 1$, then it is impossible to find a set of $|\psi'(\mathbf{r}_i)\rangle$ to complete the projection process and obtain H_{eff}. The physical picture is that, *since the YSR-type state at each lattice does not exist, the corresponding YSR-type bands cannot be formed by the hybridization of these bound states.* Thus, the topological phases from the YSR-type bands are not allowed to survive either.

D. Topological invariant and phase diagram with $0 < \gamma < 1$

Then, we consider the $0 < \gamma < 1$ case. In this case, $h_{\uparrow\uparrow,k}$ and $\Delta_{\uparrow\downarrow,k}$ are real functions about k, so one can check that $H_{\text{eff},k}$ is Hermitian.

To discuss the topological properties, we first focus on the possible gap-closing points. At $k = 0$ and $k = \pi$, Eq. (38) gives $E_{\pm,0} = M_\Delta|h_{\uparrow\uparrow,0}|$ and $E_{\pm,\pi} = M_\Delta|h_{\uparrow\uparrow,\pi}|$, and thus the first gap-closing conditions are

$$h_{\uparrow\uparrow,0} = h_{\uparrow\uparrow,\pi} = 0, \quad (40)$$

which leads to

$$\alpha_+ = 1 - \frac{1}{k_F}\left[\arctan\frac{\sin(k_F + k_h)}{e^{\frac{\sqrt{1-\gamma^2}}{\xi_0}} + \cos(k_F + k_h)}\right.$$
$$\left. + \arctan\frac{\sin(k_F - k_h)}{e^{\frac{\sqrt{1-\gamma^2}}{\xi_0}} + \cos(k_F - k_h)}\right];$$
$$\alpha_- = 1 + \frac{1}{k_F}\left[\arctan\frac{\sin(k_F + k_h)}{e^{\frac{\sqrt{1-\gamma^2}}{\xi_0}} - \cos(k_F + k_h)}\right.$$
$$\left. + \arctan\frac{\sin(k_F - k_h)}{e^{\frac{\sqrt{1-\gamma^2}}{\xi_0}} - \cos(k_F - k_h)}\right]. \quad (41)$$
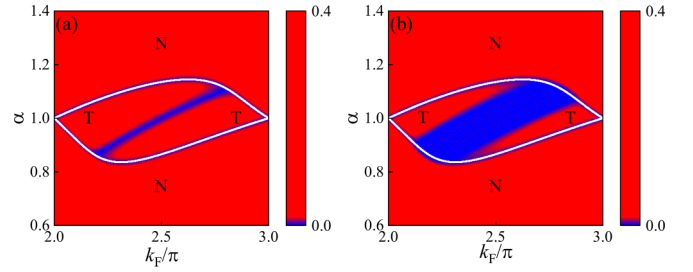
FIG. 4. Numerical results of $\min(|E_{+,k}|)$ about different k_F and α. Here $\theta = \pi/2$ in panel (a) and $\pi/3$ in panel (b). The blue (red) region denotes the (gapped) gapless regions. The label "T" ("N") represents the topological (normal) gapped phase. The white solid lines correspond to the first gap-closing condition given by Eq. (40). Other parameters are $\Delta_1 = 1.0$, $\gamma = 0$, $k_h = \pi/8$, and $\xi_0 = 2$. The result is measured in the unit of $M_\Delta = \Delta_1$.

Apart from Eq. (40), according to Eq. (38), the second gap-closing condition is that

$$\frac{1}{2}|h_{\uparrow\uparrow,k} - h_{\uparrow\uparrow,-k}| = \sqrt{\Delta_{\uparrow\downarrow,k}^2 + \frac{1}{4}(h_{\uparrow\uparrow,k} + h_{\uparrow\uparrow,-k})^2} \quad (42)$$

at a specific $k_0(k_0 \neq 0, \pi)$.

Next, we consider the topological invariant of the chain. Similar to the Kitaev chain [69], $H_{\text{eff},k}$ also satisfies the particle-hole symmetry (PHS) $\mathcal{C}H_{\text{eff},k}^T\mathcal{C}^{-1} = -H_{\text{eff},-k}^T$, with $\mathcal{C} = \tau_y$. Thus, $H_{\text{eff},k}$ with $0 < \gamma < 1$ belongs to the D class in the Hermitian Altland-Zirnbauer classification. And the corresponding topological index is $\mathbb{Z}_2$, which is given by (see Appendix E)

$$\nu = \text{sgn}(h_{\uparrow\uparrow,k=0})\text{sgn}(h_{\uparrow\uparrow,k=\pi}). \quad (43)$$

The phase boundaries are $h_{\uparrow\uparrow,k=0} = h_{\uparrow\uparrow,k=\pi} = 0$, which are exactly the first gap-closing conditions in Eq. (40).

Before discussing the effects of the non-Hermiticity, to show and review some general features [60,62] of the phase diagram, we plot the phase diagram about $k_F \in [2\pi, 3\pi]$ and α in Fig. 4. Let us begin with Fig. 4(a), which corresponds to the YSR chain with $\gamma = 0$ and $\theta = \pi/2$. We find that the first gap-closing conditions at $k = 0$ and $k = \pi$ are consistent with results given by Eq. (43). Meanwhile, the gapless phase introduced by the second gap-closing condition in Eq. (42) divides the topological phase region into two parts. Then, for Fig. 4(b) with $\gamma = 0$ and $\theta = \pi/3$, we note that the white solid lines are unchanged since the gap-closing conditions at $k = 0$ and $k = \pi$ are independent of θ [see Eqs. (40) and (41)]. The varying θ only enlarges the gapless region, separating two regions of the topological phase.

Now, we show the phase diagrams about the k_F and α with different γ and $\theta = \pi/2$ in Figs. 5(a1)–5(a3). Here we set $\xi_0 = 2$, which satisfies the short coherence length limit. Let us begin with Figs. 5(a1) and 5(a2). If $\gamma = 0.6$, the effective coherence length $\xi = \xi_0/\sqrt{1 - \gamma^2} = 1.25\xi_0$ is also in the short limit, so the two-phase diagrams are similar to each other. However, when $\gamma \lesssim 1$ (i.e., Δ_2 is comparable with Δ_1), $\xi = \xi_0/\sqrt{1 - \gamma^2} \to \infty$, and thus the phase diagram changes a lot in Fig. 5(a3). Besides, with the increasing γ, we also find that the chain with $\alpha = 1.1$ and larger k_F is more possible to be topological in Fig. 5, which is similar to the
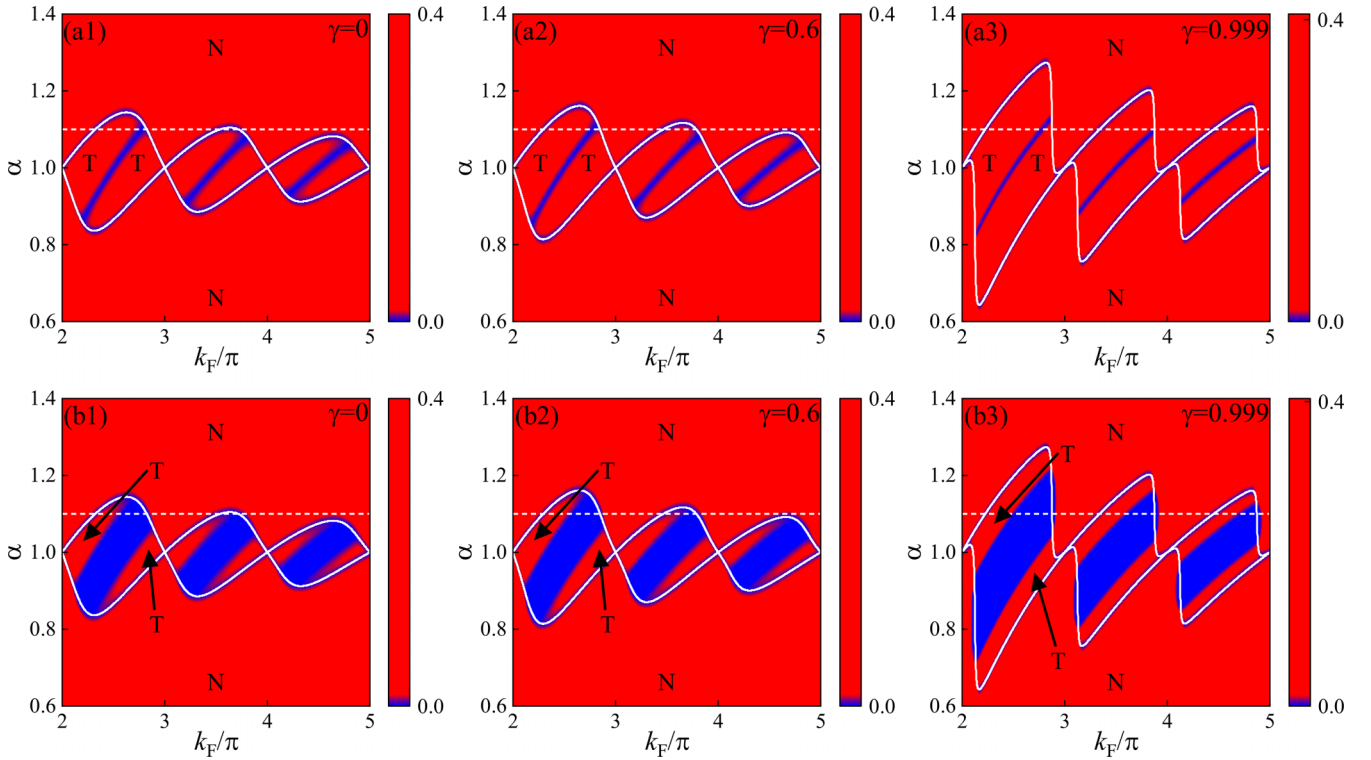
FIG. 5. Numerical results of $\min(|E_{+,k}|)$ about different k_F and α with $\gamma = 0$, 0.6, 0.999. Here, $\theta = \pi/2$ in panels (a1)–(a3) and $\pi/3$ in panels (b1)–(b3). The label "T" ("N") represents the topological (normal) gapped phase. The phase diagrams with $k_F \in [3\pi, 4\pi)$ and $k_F \in [4\pi, 5\pi)$ are similar to the one with $k_F \in [2\pi, 3\pi)$. The white solid lines correspond to the gap-closing condition given by Eq. (40). The white dashed lines are $\alpha = 1.1$. Other parameters are $\Delta_1 = 1.0$, $k_h = \pi/8$, and $\xi_0 = 2$. The result is measured in the unit of $M_\Delta = \Delta_1 \sqrt{1 - \gamma^2}$.

previous results in Ref. [62]. These results indicate that *the non-Hermitian pairing term modifies the topological phases by changing the effective coherence length* ξ. The phase diagrams with $\theta = \pi/3$ are also plotted in Figs. 5(b1)–5(b3). As we have explained, the only difference between $\theta = \pi/2$ and $\theta = \pi/3$ cases is that the gapless region dividing two topological regions is larger, which does not affect the main results. Finally, we also show the phase diagrams with different k_h in Appendix F. We find that although some details of phase diagrams are changed, the varying k_h does not change some main features of phase diagrams; e.g., each topological region is divided into two parts by a gapless region, and the phase diagrams also changes by the varying γ.

V. DISCUSSION AND SUMMARY

Now we discuss the related experimental schemes of our work. We first consider the experimental setup of the non-Hermitian s-wave superconductor with the impurity. Although the direct realization of the imbalanced s-wave superconductivity is difficult, some of our results may be still experimentally relevant: The fate of a YSR-type state depends on the effective pairing term M_Δ. Moreover, it is stimulating the imaginary pairing term M_Δ that does matter in experiments. We can, therefore, investigate the YSR-type states indirectly in related models. For instance, the YSR-type state in the transformed Hamiltonian $\tilde{H}_0(\boldsymbol{k}) = \eta H_0(\boldsymbol{k})\eta^{-1}$ in Eq. (5) could be studied in cold-atom experiments. To this end, we can use a BCS Fermi superfluid of ^{6}Li atoms with heavy ^{133}Cs

impurities. According to the accurately calibrated Feshbach resonances between ^{6}Li and ^{133}Cs [83], we can independently control the ^{133}Cs-^{6}Li scattering lengths due to the two interspecies broad resonances located near $B \approx 843$ G and 889 G, then one can realize magnetic impurity scattering by tuning the magnetic field [84,85]. As for the imaginary pairing term M_Δ, it has been pointed out that two-body losses, which have been controlled by the dissipation with photoassociation techniques [86], could lead to an imaginary s-wave pairing term [24]. Finally, it has been predicted that the polaron spectrum can be connected to the detection of Fermi superfluid excitations, including in-gap YSR states [84,85]. By combing these methods, we could confirm that the YSR-type state cannot exist in the non-Hermitian s-wave superconductor with an imaginary s-wave pairing term. Since the imaginary pairing term M_Δ also leads to the exceptional surface in our host model, one may experimentally check that the YSR-type state is forbidden to survive in our model with exceptional manifolds.

In summary, we find that the fate of the YSR-type state depends on its in-gap state nature even if the host superconductor is *non-Hermitian*: When the real part of the effective s-wave SC gap term is nonzero, the BdG gap still exists in our model. Then, we can find the YSR-type state. And the related topological phases also exist in the impurity chain. However, for the imaginary effective s-wave SC gap term, the model is in a *gapless* phase where the YSR-type states and related topological phases are not allowed to survive. Since the exceptional surfaces accompany the non-Hermitian gapless

phase, our results indicate that the non-Hermitian generation of the YSR state might have the potential to detect the exceptional surface of superconductors with the non-Hermitian s-wave pairing term in the future. Our work could be extended to the d-wave [61] or the inhomogeneous s-wave superconductor [63,64] with the non-Hermiticity. Besides, since our work only considers impurities with the classic spin, it is also valuable to investigate the interplay between quantum magnetism [87] and exceptional physics in superconductors.

APPENDIX A: LEFT EIGENSTATES AND SINGLE IMPURITY SPECTRUMS

In this Appendix, we give some details about solving the left-eigenvectors and the corresponding spectrums of the single impurity problems. The corresponding eigenequation is given by

$$[E^* - H_0^\dagger(\boldsymbol{k})]|\psi_L(\boldsymbol{r})\rangle = -gS\boldsymbol{\sigma}_n\delta(\boldsymbol{r})|\psi_L(\boldsymbol{0})\rangle. \qquad \text{(A1)}$$

With the transformation matrix in Eq. (6) of the main text, we have

$$\tilde{H}_0(\boldsymbol{k}) = \hat{\eta}^{-1}H_0^\dagger(\boldsymbol{k})\hat{\eta} = \epsilon_k\tau_z + \sqrt{\Delta_1^2 - \Delta_2^2}\,\tau_x. \qquad \text{(A2)}$$

Thus, Eq. (A1) leads to

$$\hat{\eta}^{-1}[E^* - H_0^\dagger(\boldsymbol{k})]\hat{\eta}\hat{\eta}^{-1}|\psi_L(\boldsymbol{r})\rangle = -gS\delta(\boldsymbol{r})\boldsymbol{\sigma}_n\hat{\eta}^{-1}|\psi_L(\boldsymbol{0})\rangle, \qquad \text{(A3)}$$

i.e.,

$$[E^* - \tilde{H}_0(\boldsymbol{k})]|\psi''(\boldsymbol{r})\rangle = -gS\delta(\boldsymbol{r})\boldsymbol{\sigma}_n|\psi''(\boldsymbol{r})\rangle, \qquad \text{(A4)}$$

where $|\psi''(\boldsymbol{r})\rangle = \hat{\eta}^{-1}|\psi_L(\boldsymbol{r})\rangle$. Next, by following a procedure similar to that in Eqs. (15)–(20) of the main text, we can obtain the single impurity spectrum

$$E_\pm^* = E_\pm = \pm\sqrt{\Delta_1^2 - \Delta_2^2}\frac{1-\alpha^2}{1+\alpha^2} = \pm\Delta_1\sqrt{1-\gamma^2}\frac{1-\alpha^2}{1+\alpha^2}. \qquad \text{(A5)}$$

and find that $|\psi''(\boldsymbol{r})\rangle = |\psi'(\boldsymbol{r})\rangle$. Since the Hermitian basis $|\psi'(\boldsymbol{r})\rangle$ has been given in Eq. (22) of the main text, we have the corresponding left-eigenvectors

$$|\psi_{L,+}(\boldsymbol{0})\rangle = \hat{\eta}|\psi_+'(\boldsymbol{0})\rangle = \frac{\hat{\eta}}{\sqrt{C}}\begin{pmatrix}|{\uparrow}\rangle \\ |{\uparrow}\rangle\end{pmatrix},$$

$$|\psi_{L,-}(\boldsymbol{0})\rangle = \hat{\eta}|\psi_-'(\boldsymbol{0})\rangle = \frac{\hat{\eta}}{\sqrt{C}}\begin{pmatrix}|{\downarrow}\rangle \\ -|{\downarrow}\rangle\end{pmatrix}, \qquad \text{(A6)}$$

which are exactly the results in Eq. (25) of the main text.

APPENDIX B: DERIVATION OF THE EFFECTIVE MODEL OF THE IMPURITY CHAIN

The starting model Hamiltonian in the impurity chain problem is

$$H = H_0(\boldsymbol{k}) - gS\sum_j \boldsymbol{\sigma}_{n_j}\delta(\boldsymbol{r} - \boldsymbol{r}_j). \qquad \text{(B1)}$$

According to Eq. (29) in the main text, with the transformation $\tilde{H}_0(\boldsymbol{k}) = \eta H_0(\boldsymbol{k})\eta^{-1}$ and $|\psi'(\boldsymbol{r})\rangle = \eta|\psi_R(\boldsymbol{r})\rangle = \eta^{-1}|\psi_L(\boldsymbol{r})\rangle$, we obtain the following nonlinear equation with the Hermitian YSR basis $|\psi'(\boldsymbol{r}_j)\rangle$ and the effective SC gap term M_Δ [60]:

$$[\boldsymbol{\sigma}_{n_j} + J_E(0)]|\psi'(\boldsymbol{r}_i)\rangle = -\sum_{j\neq i}(\boldsymbol{\sigma}_{n_i}\boldsymbol{\sigma}_{n_j})J_E(\boldsymbol{r}_{ij})|\psi'(\boldsymbol{r}_j)\rangle, \qquad \text{(B2)}$$

where $\boldsymbol{r}_{ij} = \boldsymbol{r}_i - \boldsymbol{r}_j$. In this nonlinear equation, $J_E(0)$ has been given in Eq. (19) of the main text, and $J_E(\boldsymbol{r})$ is [60,62]

$$J_E(\boldsymbol{r}) = -\frac{\alpha}{\sqrt{M_\Delta^2 - E^2}}\left[\frac{\sin(k_F r)e^{-\frac{\sqrt{M_\Delta^2 - E^2}}{v_F}r}}{k_F r}(E\tau_0 + M_\Delta\tau_x)\right.$$

$$\left. - \frac{\cos(k_F r)e^{-\frac{\sqrt{M_\Delta^2 - E^2}}{v_F}r}}{k_F r}\tau_z\right], \quad r > 0. \qquad \text{(B3)}$$

For $\alpha \to 1$ ($E \to 0$), expanding E to the first order makes Eq. (B2) reduce to a linear equation [60]:

$$\left[\boldsymbol{\sigma}_{n_i} - \frac{1}{M_\Delta}(E + M_\Delta\tau_x)\right]|\psi_R'(\boldsymbol{r}_i)\rangle$$

$$= \sum_{j\neq i}\frac{e^{-\frac{r_{ij}}{\xi}}}{k_F r_{ij}}[\tau_z\cos(k_F r_{ij}) + \tau_x\sin(k_F r_{ij})]\boldsymbol{\sigma}_{n_i}\boldsymbol{\sigma}_{n_j}|\psi_R'(\boldsymbol{r}_j)\rangle, \qquad \text{(B4)}$$

with $\xi = \xi_{E=0} = v_F/M_\Delta$.

Next, to obtain the effective model, we need to project Eq. (B4) to a set of $|\psi'(\boldsymbol{r}_i)\rangle$ located at impurity sites [60]. [Here, each $|\psi'(\boldsymbol{r}_i)\rangle$ is given by Eq. (22) and $|\psi'(\boldsymbol{r}_i)\rangle = \eta|\psi_R(\boldsymbol{r}_i)\rangle = \eta^{-1}|\psi_L(\boldsymbol{r}_i)\rangle$.] For the Nambu space, the nonzero inner products are

$$\langle +|\tau_x|+\rangle = 1, \quad \langle -|\tau_x|-\rangle = -1,$$
$$\langle +|\tau_z|-\rangle = 1, \quad \langle -|\tau_z|+\rangle = 1, \qquad \text{(B5)}$$

where $|\pm\rangle = \frac{1}{\sqrt{2}}(1, \pm 1)^T$. Meanwhile, the inner products in the spin space are

$$\langle \uparrow, i|\uparrow, j\rangle = \cos\frac{\theta_i}{2}\cos\frac{\theta_j}{2} + \sin\frac{\theta_i}{2}\sin\frac{\theta_j}{2}e^{-i(\phi_i - \phi_j)},$$

$$\langle \uparrow, i|\downarrow, j\rangle = e^{-i(\phi_j + \phi_i)/2}\left[\cos\frac{\theta_i}{2}\sin\frac{\theta_j}{2}e^{-i(\phi_j - \phi_i)/2}\right.$$
$$\left. - \sin\frac{\theta_i}{2}\cos\frac{\theta_j}{2}e^{-i(\phi_i - \phi_j)/2}\right]. \qquad \text{(B6)}$$

Since $\theta_j = \theta$ and $\phi_j = 2k_h x_j$ in this helical spin texture, after a unitary rotation [60], we have

$$\langle \uparrow, i|\uparrow, j\rangle = \cos^2\left(\frac{\theta}{2}\right)e^{ik_h x_{ij}} + \sin^2\left(\frac{\theta}{2}\right)e^{-ik_h x_{ij}},$$

$$\langle \uparrow, i|\downarrow, j\rangle = i\sin\theta\sin k_h x_{ij}. \qquad \text{(B7)}$$

Finally, by combing results in Eqs. (B5) and (B7), we can project a set of bases

$$[|\psi'(\boldsymbol{r}_1)\rangle, |\psi'(\boldsymbol{r}_2)\rangle, \dots, |\psi'(\boldsymbol{r}_i)\rangle, \dots, |\psi'(\boldsymbol{r}_N)\rangle\}] \qquad \text{(B8)}$$

to the nonlinear equation, Eq. (B4), and obtain the effective Hamiltonian, Eq. (31), of the main text.

APPENDIX C: FOURIER TRANSFORMATION

In this Appendix, we review the Fourier transformation in Refs. [60,62], which is used in the derivation of Eqs. (36) and (37) in the main text.

For $h_{\uparrow\uparrow}$, we need to consider the Fourier transformation like

$$
\begin{aligned}
\alpha_k &= -\sum_j \frac{\sin(k_F r_{ij})}{k_F r_{ij}} e^{-\frac{r_{ij}}{\xi}} e^{ikx_{ij}} \\
&= -\sum_{j>0} \frac{e^{i(k_F+k)j} - e^{-i(k_F+k)j} + e^{i(k_F-k)j} - e^{-i(k_F-k)j}}{2ik_F j} e^{-\frac{j}{\xi}} \\
&= -\mathrm{Im} \sum_{j>0} e^{-\frac{j}{\xi}} \frac{e^{i(k_F+k)j} + e^{i(k_F-k)j}}{j}.
\end{aligned}
\tag{C1}
$$

Here, $\xi = \xi_0/\sqrt{1-\gamma^2}$ is the effective coherence length. Then, when the length of the impurity chain $L \to \infty$, we can use the identity

$$
-\ln(1-x) = \sum_{j>0}^{\infty} \frac{x^j}{j}
\tag{C2}
$$

and obtain

$$
\alpha_k = \mathrm{Im}\left[\ln\left(1 - e^{-\frac{1}{\xi}} e^{i(k_F+k)}\right) + \ln\left(1 - e^{-\frac{1}{\xi}} e^{i(k_F-k)}\right)\right].
\tag{C3}
$$

Since $\mathrm{Im}\ln z = \arctan\frac{\mathrm{Im}z}{\mathrm{Re}z}$, we have

$$
\begin{aligned}
\alpha_k &= -\left[\arctan\frac{e^{-\frac{1}{\xi}}\sin(k_F+k)}{1 - e^{-\frac{1}{\xi}}\cos(k_F+k)} \right. \\
&\quad \left. + \arctan\frac{e^{-\frac{1}{\xi}}\sin(k_F-k)}{1 - e^{-\frac{1}{\xi}}\cos(k_F-k)} \right] \\
&= -\left[\arctan\frac{\sin(k_F+k)}{e^{\frac{1}{\xi}} - \cos(k_F+k)} \right. \\
&\quad \left. + \arctan\frac{\sin(k_F-k)}{e^{\frac{1}{\xi}} - \cos(k_F-k)} \right].
\end{aligned}
\tag{C4}
$$

Then we have Eq. (36) in the main text.

As for $\Delta_{\uparrow\downarrow}$, its Fourier transformation is as follows:

$$
\begin{aligned}
\Delta_{\uparrow\downarrow,k} &= i\sin\theta \sum_j \frac{\cos(k_F r_{ij}) e^{-\frac{r_{ij}}{\xi}}}{k_F r_{ij}} \sin(k_h x_{ij}) e^{ikx_{ij}} \\
&= \frac{\sin\theta}{4k_F} \sum_j \frac{(e^{ik_F r_{ij}} + e^{-ik_F r_{ij}}) e^{-\frac{r_{ij}}{\xi}}}{r_{ij}} \\
&\quad \times [e^{i(k_h+k)x_{ij}} - e^{i(k-k_h)x_{ij}}] \\
&= \frac{\sin\theta}{4k_F} \sum_{j>0} \frac{(e^{ik_F j} + e^{-ik_F j}) e^{-\frac{j}{\xi}}}{j} \\
&\quad \times [e^{i(k_h+k)j} - e^{i(k-k_h)j} + e^{-i(k_h+k)j} - e^{-i(k-k_h)j}]
\end{aligned}
$$

$$
\begin{aligned}
&= \frac{\sin\theta}{4k_F} \sum_{j>0} \frac{e^{-\frac{j}{\xi}}}{j} [(e^{i(k_F+k_h+k)j} - e^{i(k_F+k_h-k)j} \\
&\quad - e^{i(k_F-k_h+k)j} + e^{i(k_F-k_h-k)j}) + \mathrm{c.c.}].
\end{aligned}
\tag{C5}
$$

Note that Eq. (C5) includes the following summation:

$$
\begin{aligned}
\beta_k &= \sum_{j>0} \frac{e^{-\frac{j}{\xi}}}{j}(e^{ikj} + \mathrm{c.c.}) \\
&= -\ln\left[1 - e^{i(k+\frac{i}{\xi})}\right] - \ln\left[1 - e^{-i(k-\frac{i}{\xi})}\right] \\
&= -\ln\left(1 + e^{-\frac{2}{\xi}} - 2e^{-\frac{1}{\xi}}\cos k\right),
\end{aligned}
\tag{C6}
$$

we have

$$
\Delta_{\uparrow\downarrow,k} = \frac{\sin\theta}{4k_F}(\beta_{k_F+k_h+k} - \beta_{k_F+k_h-k} - \beta_{k_F-k_h+k} + \beta_{k_F-k_h-k}),
\tag{C7}
$$

which is exactly Eq. (37) in the main text.

APPENDIX D: $H_{\mathrm{eff},k}$ WITH THE $\gamma > 1$ CASE

In this Appendix, we investigate $H_{\mathrm{eff},k}$ with the $\gamma > 1$ case. Before discussing this Hamiltonian, we have to stress that since the single YSR-type state cannot exist in the $\gamma > 1$ case, $H_{\mathrm{eff},k}$ cannot be obtained by overlapping YSR-type states. Here, the results of the $\gamma > 1$ case are discussed only to make comparisons with ones of the $0 \leqslant \gamma < 1$ case. And we set $(\alpha, k_F, k_h, \theta) = (1.11, 2.5\pi, 0.125\pi, 0.5\pi)$ in this Appendix.

For $H_{\mathrm{eff},k}$ with $\gamma > 1$ cases, one can check that the PHS $\mathcal{C}H_{\mathrm{eff},k}^T\mathcal{C}^{-1} = -H_{\mathrm{eff},-k}^T$, with $\mathcal{C} = \tau_y$, is also satisfied. According to the non-Hermitian Altland-Zirnbauer class, the topological invariant can be given by the following $\mathcal{Z}_2$ index [88]:

$$
\begin{aligned}
\nu' &= \mathrm{sgn}(R) \\
&= \mathrm{sgn}\left\{ \frac{\mathrm{Pf}(H_{\mathrm{eff},\pi}\mathcal{C})}{\mathrm{Pf}(H_{\mathrm{eff},0}\mathcal{C})} \exp\left[-\frac{1}{2}\int_{k=0}^{k=\pi} d\ln\det(H_{\mathrm{eff},k}\mathcal{C}) \right] \right\},
\end{aligned}
\tag{D1}
$$

which is valid for models with both line and point gaps. Since the $\mathcal{Z}_2$ index is determined by the sign of R, this topological invariant is ill-defined if R has a nonzero imaginary part. In Fig. 6(a), we show real and imaginary parts of R with varying $\gamma \in [0, 1) \cup (1, 1.5]$ ($H_{\mathrm{eff},k}$ with $\gamma = 1$ is just a trivial zero-matrix). For $\gamma \in [0, 1)$, the *real* number $R = -1$, and thus the $\mathcal{Z}_2$ index in Eq. (D1) is well-defined. The system is in the topological phase, which is consistent with the results given by Eq. (43) in the main text. When $\gamma \in (1, 1.5]$, the imaginary part of R can be nonzero, and then the $\mathcal{Z}_2$ index is ill-defined.

To support the result in Fig. 6(a), we also calculate the local density of state (LDOS), which is given by

$$
\begin{aligned}
A(j, \omega) &= -\frac{1}{\pi}\mathrm{Im}[G_{p,j}(\omega) + G_{h,j}(\omega)], \\
G(\omega) &= \lim_{\delta \to 0^+} \frac{1}{\omega - H_{\mathrm{eff}} + i\delta}.
\end{aligned}
\tag{D2}
$$
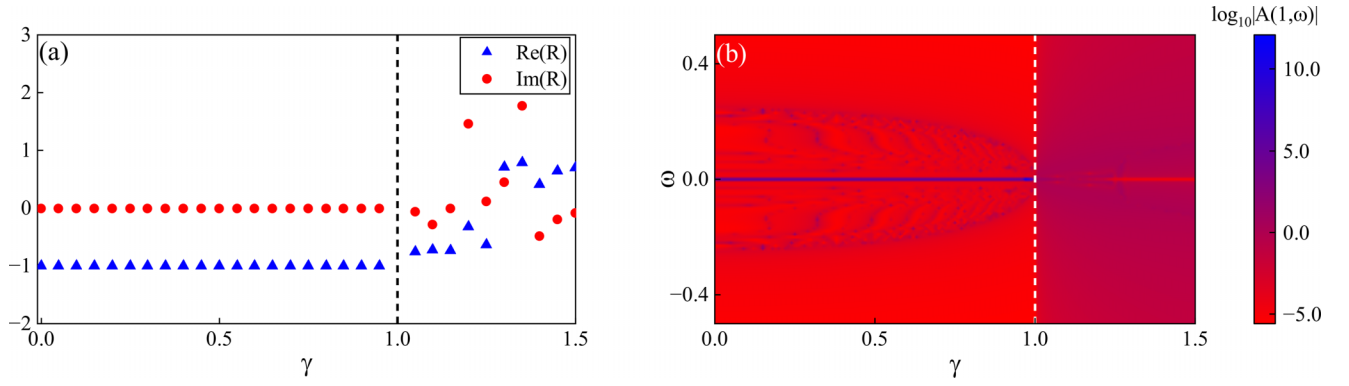
FIG. 6. (a) Re(R) and Im(R) as functions of γ. (b) The LDOS at the first site of the impurity chain. The black and white dashed lines are $\gamma = 1.0$. Other parameters are $\Delta_1 = 1.0$, $k_h = \pi/8$, $k_F = 5\pi/2$, $\theta = \pi/2$, $\alpha = 1.11$, $\delta = 10^{-6}$, the number of impurity sites $N = 100$, and $\xi_0 = 2$.

Here p (h) denotes the particle (hole) space, and j represents the jth site of the impurity chain. In Fig. 6(b) we show $\log_{10} |A(1, \omega)|$ as a function of γ and ω. For $\omega = 0$, as the $\gamma \in [0, 1)$, we find that the scale of $A(1, \omega = 0)$ is much larger, which means that topological zero modes exist and they localize at the boundary. When $\gamma \in (1, 1.5]$, $\log_{10} |A(1, \omega)|$ sharply decreases, which means that topological boundary modes do not exist, and the system is not topological.

APPENDIX E: SOME DETAILS OF DERIVING THE $\mathcal{Z}_2$ TOPOLOGICAL INVARIANTS

In this Appendix, we show some details about deriving the $\mathcal{Z}_2$ topological invariants. For the Hamiltonian

$$
\begin{aligned}
H_{\mathrm{eff},k} = {} & \frac{M_\Delta}{2}(h_{\uparrow\uparrow,k} + h_{\uparrow\uparrow,-k})\tau_z + M_\Delta \Delta_{\uparrow\uparrow,k}\tau_x \\
& + \frac{M_\Delta}{2}(h_{\uparrow\uparrow,k} - h_{\uparrow\uparrow,-k})\tau_0.
\end{aligned} \tag{E1}
$$
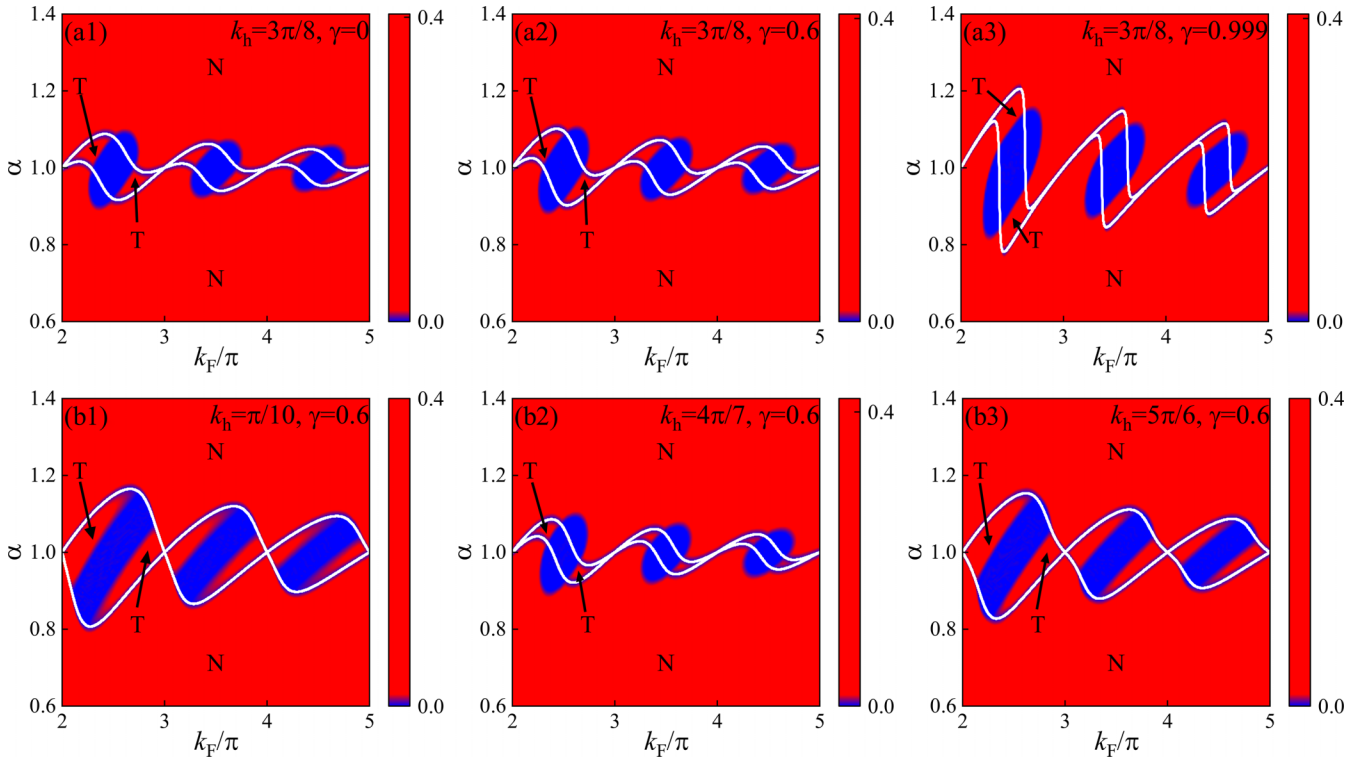
FIG. 7. Numerical results of $\min(|E_{+,k}|)$ about different k_F and α. (a1)–(a3): Results with $k_h = 3\pi/8$ and $\gamma = 0$, 0.6, and 0.999. (b1)–(b3): Results with $k_h = \pi/10$, $4\pi/7$, and $5\pi/6$ and $\gamma = 0.6$. The label "T" ("N") represents the topological (normal) gapped phase. The phase diagrams with $k_F \in [3\pi, 4\pi)$ and $k_F \in [4\pi, 5\pi)$ are similar to the one with $k_F \in [2\pi, 3\pi)$. The white solid lines correspond to the first gap-closing condition, Eq. (40). Other parameters are $\Delta_1 = 1.0$, $\theta = \pi/3$, and $\xi_0 = 2$. The black regions denote the phases with the negative gap term, which are also gapless phases. The result is measured in the unit of $M_\Delta = \Delta_1\sqrt{1 - \gamma^2}$.

After the following unitary transformation,

$$U = \frac{1}{\sqrt{2}}\begin{pmatrix} 1 & 1 \\ -i & i \end{pmatrix}, \tag{E2}$$

we have $\tilde{H}_{\text{eff},k} = U H_{\text{eff},k} U^\dagger = iA_k$, with

$$A_k = M_\Delta \begin{pmatrix} -i\Delta_{\uparrow\uparrow,k} - \frac{i}{2}(h_{\uparrow\uparrow,k} - h_{\uparrow\uparrow,-k}) & \frac{1}{2}(h_{\uparrow\uparrow,k} + h_{\uparrow\uparrow,-k}) \\ -\frac{1}{2}(h_{\uparrow\uparrow,k} + h_{\uparrow\uparrow,-k}) & i\Delta_{\uparrow\uparrow,k} - \frac{i}{2}(h_{\uparrow\uparrow,k} - h_{\uparrow\uparrow,-k}) \end{pmatrix}. \tag{E3}$$

According to Eqs. (36) and (37) of the main text, we can check that $(h_{\uparrow\uparrow,k} - h_{\uparrow\uparrow,-k}) = \Delta_{\uparrow\uparrow,k} = 0$ when $k = 0$ and $k = -\pi$, which leads to $A_0 = -A_0^T$ and $A_\pi = -A_\pi^T$. Note that we consider the $0 < \gamma < 1$ case and $\Delta_1 > 0$, and we have $M_\Delta = \Delta_1\sqrt{1-\gamma^2} > 0$. Thus, we can calculate the following $\mathcal{Z}_2$ topological invariant at $k = 0$ and $k = -\pi$ [69] by Pfaffian:

$$\nu = \text{sgn}[\text{Pf}(A_0)]\text{sgn}[\text{Pf}(A_\pi)] = \text{sgn}(h_{\uparrow\uparrow,k=0})\text{sgn}(h_{\uparrow\uparrow,k=\pi}), \tag{E4}$$

which is exactly Eq. (43) in the main text.

APPENDIX F: PHASE DIAGRAMS WITH A VARYING k_h

In this Appendix, we show phase diagrams with a fixed $\theta = \pi/3$ and varying k_h and γ in Fig. 7. In Figs. 7(a1)–7(a3), we set $k_h = 3\pi/8$ and change γ. Then, one can find that the different $k_h = 3\pi/8$ only introduces the phase with $\min(E_{\pm,k}) < 0$, which also belongs to the gapless phase, and the phase diagrams still change according to the varying γ. Next, after setting $\gamma = 0.6$ and changing k_h, Figs. 7(b1)–7(b3) show that the varying k_h modifies the gapless regions given by the gap-closing conditions, Eqs. (40) and (42). However, although some details of phase diagrams are changed, the key feature that the topological regions are separated by the gapless region still exists in Fig. 7.

[1] Y. Ashida, Z. Gong, and M. Ueda, Adv. Phys. **69**, 249 (2020).

[2] E. J. Bergholtz, J. C. Budich, and F. K. Kunst, Rev. Mod. Phys. **93**, 015005 (2021).

[3] V. Kozii and L. Fu, arXiv:1708.05841.

[4] C. M. Bender and S. Boettcher, Phys. Rev. Lett. **80**, 5243 (1998).

[5] C. M. Bender, Rep. Prog. Phys. **70**, 947 (2007).

[6] A. Cerjan, M. Xiao, L. Yuan, and S. Fan, Phys. Rev. B **97**, 075128 (2018).

[7] H.-Q. Wang, J.-W. Ruan, and H.-J. Zhang, Phys. Rev. B **99**, 075130 (2019).

[8] V. V. Konotop, J. Yang, and D. A. Zezyulin, Rev. Mod. Phys. **88**, 035002 (2016).

[9] R. Okugawa and T. Yokoyama, Phys. Rev. B **99**, 041202(R) (2019).

[10] L. Feng, R. El-Ganainy, and L. Ge, Nat. Photonics **11**, 752 (2017).

[11] R. El-Ganainy, K. G. Makris, M. Khajavikhan, Z. H. Musslimani, S. Rotter, and D. N. Christodoulides, Nat. Phys. **14**, 11 (2018).

[12] M. Kulishov, J. M. Laniel, N. Bélanger, J. Azaña, and D. V. Plant, Opt. Express **13**, 3068 (2005).

[13] S. Longhi, J. Phys. A: Math. Theor. **44**, 485302 (2011).

[14] L. Feng, Z. J. Wong, R.-M. Ma, Y. Wang, and X. Zhang, Science **346**, 972 (2014).

[15] M. Papaj, H. Isobe, and L. Fu, Phys. Rev. B **99**, 201107(R) (2019).

[16] E. J. Bergholtz and J. C. Budich, Phys. Rev. Res. **1**, 012003(R) (2019).

[17] Y. Nagai, Y. Qi, H. Isobe, V. Kozii, and L. Fu, Phys. Rev. Lett. **125**, 227204 (2020).

[18] T. Yoshida, R. Peters, and N. Kawakami, Phys. Rev. B **98**, 035141 (2018).

[19] J. Carlström and E. J. Bergholtz, Phys. Rev. A **98**, 042114 (2018).

[20] P.-L. Zhao, A.-M. Wang, and G.-Z. Liu, Phys. Rev. B **98**, 085150 (2018).

[21] H. Zhou, C. Peng, Y. Yoon, C. W. Hsu, K. A. Nelson, L. Fu, J. D. Joannopoulos, M. Soljčać, and B. Zhen, Science **359**, 1009 (2018).

[22] H. Wu and J.-H. An, Phys. Rev. B **105**, L121113 (2022).

[23] R. Schäfer, J. C. Budich, and D. J. Luitz, Phys. Rev. Res. **4**, 033181 (2022).

[24] K. Yamamoto, M. Nakagawa, K. Adachi, K. Takasan, M. Ueda, and N. Kawakami, Phys. Rev. Lett. **123**, 123601 (2019).

[25] R. Hanai and P. B. Littlewood, Phys. Rev. Res. **2**, 033018 (2020).

[26] J. Li, A. K. Harter, J. Liu, L. de Melo, Y. N. Joglekar, and L. Luo, Nat. Commun. **10**, 855 (2019).

[27] Y. Xu, S.-T. Wang, and L.-M. Duan, Phys. Rev. Lett. **118**, 045701 (2017).

[28] S. Malzard, C. Poli, and H. Schomerus, Phys. Rev. Lett. **115**, 200402 (2015).

[29] T. E. Lee and C.-K. Chan, Phys. Rev. X **4**, 041001 (2014).

[30] S. Diehl, E. Rico, M. A. Baranov, and P. Zoller, Nat. Phys. **7**, 971 (2011).

[31] Y. Choi, S. Kang, S. Lim, W. Kim, J.-R. Kim, J.-H. Lee, and K. An, Phys. Rev. Lett. **104**, 153601 (2010).

[32] F. Tonielli, J. C. Budich, A. Altland, and S. Diehl, Phys. Rev. Lett. **124**, 240404 (2020).

[33] P. He and Z. H. Huang, Phys. Rev. A **102**, 062201 (2020).

[34] Y. Michishita, T. Yoshida, and R. Peters, Phys. Rev. B **101**, 085122 (2020).

[35] C. Lehmann, M. Schüler, and J. C. Budich, Phys. Rev. Lett. **127**, 106601 (2021).

[36] K. Kimura, T. Yoshida, and N. Kawakami, Phys. Rev. B **100**, 115124 (2019).

[37] A. A. Zyuzin and A. Yu. Zyuzin, Phys. Rev. B **97**, 041203(R) (2018).

[38] R. Aquino and D. G. Barci, Phys. Rev. B **104**, 195150 (2021).

[39] R. Rausch, R. Peters, and T. Yoshida, New J. Phys. **23**, 013011 (2021).

[40] J. Avila, F. Peñaranda, E. Prada, P. San-Jose, and R. Aguado, Commun. Phys. **2**, 133 (2019).

[41] K. Moors, A. A. Zyuzin, A. Y. Zyuzin, R. P. Tiwari, and T. L. Schmidt, Phys. Rev. B **99**, 041116(R) (2019).

[42] A. A. Zyuzin and P. Simon, Phys. Rev. B **99**, 165145 (2019).

[43] A. Cerjan, S. Huang, M. Wang, K. P. Chen, Y. Chong, and M. C. Rechtsman, Nat. Photonics **13**, 623 (2019).

[44] Ş. K. Özdemir, S. Rotter, F. Nori, and L. Yang, Nat. Mater. **18**, 783 (2019).

[45] K. Wang, L. Xiao, J. C. Budich, W. Yi, and P. Xue, Phys. Rev. Lett. **127**, 026404 (2021).

[46] Q. Liu, S. Li, B. Wang, S. Ke, C. Qin, K. Wang, W. Liu, D. Gao, P. Berini, and P. Lu, Phys. Rev. Lett. **124**, 153903 (2020).

[47] L. Feng, Y. L. Xu, W. S. Fegadolli, M. H. Lu, J. E. B. Oliveira, V. R. Almeida, Y. F. Chen, and A. Scherer, Nat. Mater. **12**, 108 (2013).

[48] H. Hodaei, A. U. Hassan, S. Wittek, H. Garcia-Gracia, R. El-Ganainy, D. N. Christodoulides, and M. Khajavikhan, Nature (London) **548**, 187 (2017).

[49] W. Chen, K. Özdemir, G. Zhao, J. Wiersig, and L. Yang, Nature (London) **548**, 192 (2017).

[50] B. Peng, K. Özdemir, F. Lei, F. Monifi, M. Gianfreda, G. L. Long, S. Fan, F. Nori, C. M. Bender, and L. Yang, Nat. Phys. **10**, 394 (2014).

[51] H. Hodaei, M.-A. Miri, M. Heinrich, D. N. Christodoulides, and M. Khajavikhan, Science **346**, 975 (2014).

[52] J. Doppler, A. A. Mailybaev, J. Böhm, U. Kuhl, A. Girschik, F. Libisch, T. J. Milburn, P. Rabl, N. Moiseyev, and S. Rotter, Nature (London) **537**, 76 (2016).

[53] J. Friedel, Lond. Edinb. Dublin Philos. Mag. J. Sci. **43**, 153 (1952).

[54] J. Friedel, Nuovo Cim. **7**, 287 (1958).

[55] L. Yu, Acta Phys. Sin. **21**, 75 (1965).

[56] H. Shiba, Prog. Theor. Phys. **40**, 435 (1968).

[57] A. I. Rusinov, JETP Lett. **9**, 85 (1969).

[58] T.-P. Choy, J. M. Edge, A. R. Akhmerov, and C. W. J. Beenakker, Phys. Rev. B **84**, 195442 (2011).

[59] S. Nadj-Perge, I. K. Drozdov, B. A. Bernevig, and A. Yazdani, Phys. Rev. B **88**, 020407(R) (2013).

[60] F. Pientka, L. I. Glazman, and F. von Oppen, Phys. Rev. B **88**, 155420 (2013).

[61] M. Mashkoori and A. Black-Schaffer, Phys. Rev. B **99**, 024505 (2019).

[62] A. Weström, K. Pöyhönen, and T. Ojanen, Phys. Rev. B **91**, 064502 (2015).

[63] A. A. Bespalov, Phys. Rev. B **100**, 094507 (2019).

[64] S. Hoffman, J. Klinovaja, and D. Loss, Phys. Rev. B **93**, 165418 (2016).

[65] K. Pöyhönen, A. Weström, J. Röntynen, and T. Ojanen, Phys. Rev. B **89**, 115109 (2014).

[66] P. M. R. Brydon, S. Das Sarma, H. Y. Hui, and J. D. Sau, Phys. Rev. B **91**, 064505 (2015).

[67] S. Nadj-Perge, I. K. Drozdov, J. Li, H. Chen, S. Jeon, J. Seo, A. H. MacDonald, B. A. Bernevig, and A. Yazdani, Science **346**, 602 (2014).

[68] B. E. Feldman, M. T. Randeria, J. Li, S. Jeon, Y. Xie, Z. Wang, I. K. Drozdov, B. A. Bernevig, and A. Yazdani, Nat. Phys. **13**, 286 (2017).

[69] A. Y. Kitaev, Phys.-Usp. **44**, 131 (2001).

[70] J. Alicea, Rep. Prog. Phys. **75**, 076501 (2012).

[71] M. Z. Hasan and C. L. Kane, Rev. Mod. Phys. **82**, 3045 (2010).

[72] X.-L. Qi and S. C. Zhang, Rev. Mod. Phys. **83**, 1057 (2011).

[73] M. Sato and S. Fujimoto, J. Phys. Soc. Jpn. **85**, 072001 (2016).

[74] R. M. Lutchyn, J. D. Sau, and S. Das Sarma, Phys. Rev. Lett. **105**, 077001 (2010).

[75] Y. Oreg, G. Refael, and F. von Oppen, Phys. Rev. Lett. **105**, 177002 (2010).

[76] A. Ghatak and T. Das, Phys. Rev. B **97**, 014512 (2018).

[77] C. Li, X. Z. Zhang, G. Zhang, and Z. Song, Phys. Rev. B **97**, 115436 (2018).

[78] V. Kornich and B. Trauzettel, Phys. Rev. Res. **4**, L022018 (2022).

[79] V. Kornich and B. Trauzettel, Phys. Rev. Res. **4**, 033201 (2022).

[80] X. M. Zhao, C. X. Guo, S. P. Kou, L. Zhuang, and W. M. Liu, Phys. Rev. B **104**, 205131 (2021).

[81] X. M. Zhao, C. X. Guo, M. L. Yang, H. Wang, W. M. Liu, and S. P. Kou, Phys. Rev. B **104**, 214502 (2021).

[82] For the single impurity problem, this intergral is completed in the inteval $\epsilon_k \in [-\omega_D, \omega_D]$ (ω_D is the Debye frequency) near the Fermi level E_F, and we consider the limit with $E_F, \omega_D \to \infty$, while keeping $\omega_D/E_F << 1$.

[83] S.-K. Tung, C. Parker, J. Johansen, C. Chin, Y. Wang, and P. S. Julienne, Phys. Rev. A **87**, 010702(R) (2013).

[84] J. Wang, X.-J. Liu, and H. Hu, Phys. Rev. Lett. **128**, 175301 (2022).

[85] J. Wang, X.-J. Liu, and H. Hu, Phys. Rev. A **105**, 043320 (2022).

[86] T. Tomita, S. Nakajima, I. Danshita, Y. Takasu, and Y. Takahashi, Sci. Adv. **3**, e1701513 (2017).

[87] J. F. Steiner, C. Mora, K. J. Franke, and F. von Oppen, Phys. Rev. Lett. **128**, 036801 (2022).

[88] K. Kawabata, K. Shiozaki, M. Ueda, and M. Sato, Phys. Rev. X **9**, 041015 (2019).